Ionization Chamber Measurements of the Absorption of the N-Component of Cosmic Rays in Lead*

H. S. BRIDGE AND R. H. REDIKER
Department of Physics and Laboratory for Nuclear Science and Engineering, Massachusetts Institute of Technology, Cambridge, Massachusetts
(Received May 15, 1952)

A detecting system that responds only to ionization bursts produced by nuclear interactions of the so-called N-component of cosmic radiation is described. The burst rate observed with this detector has been measured as a function of the thickness of lead absorber above the system at sea level and at 10,600 feet.

The absorption of the N-component in lead cannot be represented by an exponential variation of the intensity with absorber thickness; instead the "absorption curve" shows an initial increase in intensity. This behavior may be explained by the assumption that π-mesons with energies of several Bev, which are produced in the nuclear interactions, can give rise to further nuclear interactions.

From the altitude variation of the smallest recorded bursts produced by the N-component, one finds a value of 119 ± 5 g cm^{-2} for the absorption thickness of the producing radiation in air. The absorption thickness decreases with increasing energy of the nuclear event detected.

In the same experiment, other kinds of events were also recorded, which could be produced either by N-rays or by μ-mesons. The bursts produced by these two components were separated on the basis of the experimental altitude variation of N-rays and of the computed altitude variation of the μ-meson induced bursts. For our particular ionization chamber about 50 percent of the bursts at sea level produced by charged particles incident on the 219 g cm^{-2} lead ionization chamber shield were caused by μ-mesons and 50 percent by the N-component.

I. INTRODUCTION

THE results reported in this paper were obtained in a continuation of previous experiments[1–5] performed with a lead-shielded ionization chamber and an array of Geiger-Mueller counters above the lead shield. The time coincident pulses of the ionization chamber and of the Geiger counters recorded the arrival of penetrating ionizing particles which could produce ionization bursts below the lead shield. Measurements with this type of detector established the variation of the ionization burst rate with altitude and led to the conclusion that at airplane altitudes most of the observed bursts arise from nuclear interactions of the so-called N-component, while at sea level most of the bursts arise from electromagnetic interactions of μ-mesons.[4] From measurements made at 14,300 feet, the absorption of the burst-producing radiation in lead turned out to be much greater than that of the penetrating component of cosmic rays, but smaller than that corresponding to the geometric cross section of the lead nuclei.

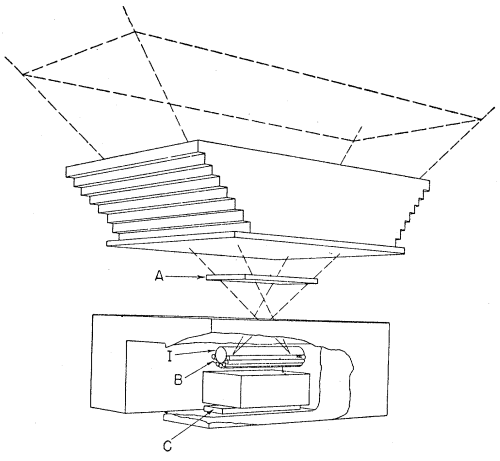

FIG. 1(a). Perspective view of experimental arrangement showing full 455 g cm^{-2} lead absorber as stacked at sea level. For greater clarity the 57 g cm^{-2} of lead in Σ' have been omitted.

As stated above the bursts observed in the ionization chamber are caused either by μ-mesons or nucleons which interact in the shielding material above the chamber. While the first case is well understood, the processes by which nuclear interactions produce ionization bursts are only understood qualitatively. All the charged products contribute to the total ionization but the relative contributions from different products are unknown. However, at energies of several Bev the ionization caused by electron cascades is important. Probably these cascades originate from the decay photons of neutral π-mesons.

Under the assumption that all bursts result from electron cascades initiated by single electrons or photons, a detector such as that described above has some important properties. For a given number of electrons at the chamber there corresponds a minimum initiating energy at a unique position in the shield above the chamber. For our detector the absolute minimum energy transfer required is 3.2 Bev and occurs 48 g cm^{-2} of lead above the chamber.[6] Because

* This work was supported in part by the joint program of the ONR and AEC.

[1] Bridge, Rossi, and Williams, Phys. Rev. **72**, 257 (1947).
[2] Bridge, Hazen, and Rossi, Phys. Rev. **73**, 179 (1948).
[3] Bridge, Hazen, Rossi, and Williams, Phys. Rev. **74**, 1083 (1948).
[4] H. Bridge and B. Rossi, Phys. Rev. **75**, 810 (1949).
[5] McMahon, Rossi, and Burditt, Phys. Rev. **80**, 157 (1950).

[6] These values are obtained from the computations of J. Belenky, J. Phys. (U.S.S.R.) **8**, 305 (1944). The smallest detected burst corresponded to 16 electrons of 10 Mev passing through the chamber perpendicular to its axis. Since many of the electrons in the electronic cascade in the lead are scattered at large angles, sixteen electrons passing through the chamber has been assumed to correspond to a shower of 32 electrons in the lead directly above the chamber. See the appendix for a discussion of the validity of this assumption.

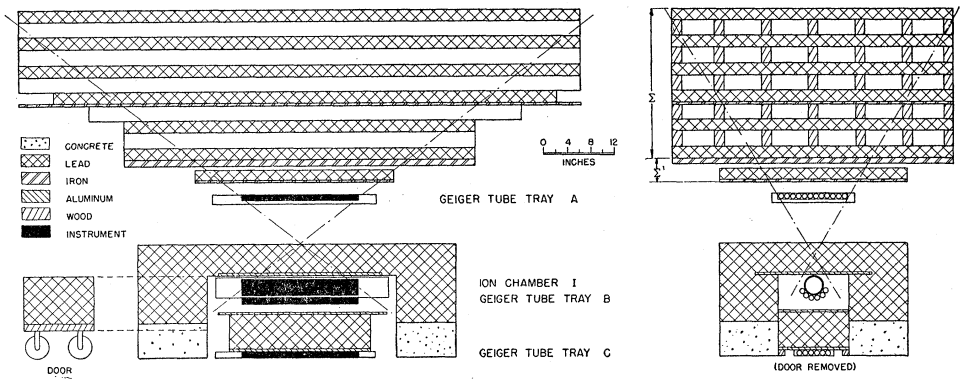

FIG. 1(b). Side and front views of experimental arrangement showing the full 341 g cm^{-2} lead absorber as stacked at 10,600 feet.

the main contribution to the shower rate comes from the lowest energy transfers that can produce the observed effects, the interactions responsible for the ionization bursts are localized mainly in this vicinity.[7] This is important if it is desirable to define a zero thickness of absorber.

In the present experiment, performed at sea level and at 10,600 feet, we have attempted to separate the bursts produced by μ-mesons (to be called μ-bursts) from those produced by the N-component (to be called N-bursts). We have made more accurate measurements of the absorption in air and in lead of the burst-producing radiation and have also tried to determine the collision mean free path for the N-component in lead.

II. EXPERIMENTAL ARRANGEMENT

The experimental arrangement is shown in Fig. 1. The ionization chamber, I, was of the type described previously.[3] It had a diameter of 7.5 cm and an effective length of 52 cm. The chamber used at sea level was filled with purified argon at 7.3 atmospheres (25°C) and contained a fixed source of polonium α-particles placed near the inner surface of the cylindrical wall. The chamber used at 10,600 feet was similar physically but was filled with argon at 7.1 atmospheres (25°C) and contained a removable source of polonium α-particles placed near the inner surface of the cylindrical wall. Tests comparing the counting rates of the two chambers for electron showers showed that for the same number of electrons traversing the chamber the pulses of the chamber used at sea level were 10 percent greater than those of the chamber used at 10,600 feet. The minimum pulse height required from the chambers was 0.3 times that of an α-particle pulse.

A tray of Geiger-Mueller counters, A, was placed above the ionization chamber and was separated from it by 142 g cm^{-2} of lead. This lead served as the producing layer for most of the bursts observed in the ionization chamber. Immediately below the chamber there was a second tray of counters, B. Below tray B and separated from it by 171 g cm^{-2} of lead there was a third tray of counters, C. All counters had diameters of 2.5 cm and effective lengths of 51 cm.

Above tray A one could place an absorber Σ' consisting of 57 g cm^{-2} of lead and 20 g cm^{-2} of iron. Above Σ' one could stack different thicknesses of lead to form the absorber Σ. At sea level the lead in Σ was stacked solid as shown in Fig. 1(a). At 10,600 feet, however, wooden spacers were placed between the layers in lead in Σ as shown in Fig. 1(b). This arrangement facilitated the comparison between absorption measurements in lead and absorption measurements in carbon. The latter will be described in a subsequent paper.

A block diagram of the electronic circuits as used at 10,600 feet is shown in Fig. 2. An electronic discriminator selected pulses of different heights from the

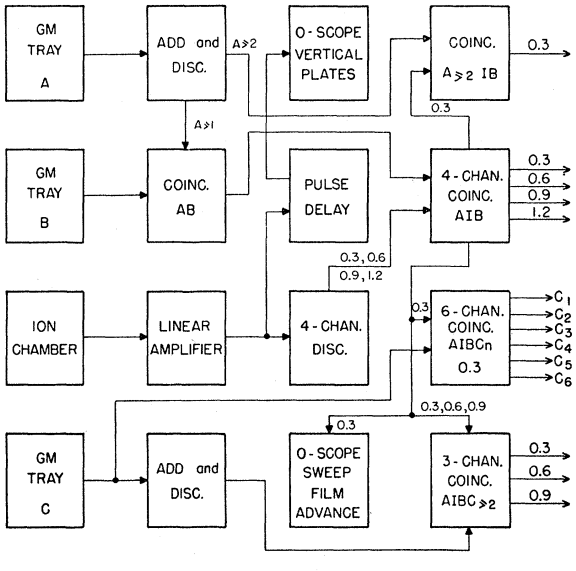

FIG. 2. Simplified block diagram of the equipment. The signal level of the ionization chamber pulse is indicated at appropriate points. Pulse-height discriminators are shown by the abbreviation DISC. Only the more important coincidence outputs which were connected to the Esterline-Angus recorder are given. Pulse shaping circuits are not shown, but all pulses were shaped to be rectangular and 20 μ-seconds wide. At sea level it was not possible to determine whether more than one tube in tray A was discharged but only whether one or both halves of the tray were struck.

[7] See appendix.

TABLE I. The coincidences whose rates were investigated as a function of absorber thickness.

AI	Coincidence between pulse in Geiger Tray A and ionization burst in chamber.
AIB	Coincidence between pulses in Geiger Trays A and B and ionization burst in chamber.
A_1IB	Same as AIB except that only one Geiger tube in Tray A was struck.
$AIBC$	Coincidence between pulses in Geiger Trays A, B, and C and ionization burst in chamber.
A_1IBC	Same as $AIBC$ except that only one Geiger tube in Tray A was struck.
$AIBC_0$	Coincidence between pulses in Geiger Trays A and B and ionization burst in chamber, in anticoincidence with pulse from Tray C.
A_1IBC_0	Same as $AIBC_0$ except that only one Geiger tube in Tray A was struck.
$AIBC_1$	Same as $AIBC$ except that only one Geiger tube in Tray C was struck.
A_1IBC_1	Same as $AIBC$ except that only one Geiger tube in each of the Trays A and C were struck.
$AIBC_2$	Same as $AIBC$ except that at least two Geiger tubes in Tray C were struck (denoted by $AIBC\geqq_2$ in the figures).
A_1IBC_2	Same as $AIBC$ except that at least two Geiger tubes in Tray C were struck and only one Geiger tube in Tray A was struck (denoted by $A_1IBC\geqq_2$ in the figures).

The size of voltage pulses from the ionization chamber is given in terms of the voltage pulse caused by a polonium α-particle (5.30 Mev) near the wall of the chamber. The relative size is indicated by the subscript following I. I_m means the voltage due to the ionization burst was larger than m times the pulse due to the polonium α-particle.

ionization chamber and addition circuits followed by pulse-height discriminators selected events where more than certain predetermined numbers of counters in individual trays were discharged. Various types of coincidences were then recorded electronically. In addition, certain types of coincidences were analyzed by means of a 20-pen Esterline-Angus recorder, giving detailed information on the number of counters discharged in tray A, the number and position of the counters discharged in tray C, and the size of the ionization burst.

Requiring a coincidence between the ionization chamber I and a counter in tray B excluded low energy interactions whose secondary particles failed to emerge from the wall of the ionization chamber. Requiring a coincidence between I and more than one C counter insured that the event causing the ionization burst in I was one in which penetrating particles were produced. In this manner one could eliminate showers resulting from electromagnetic interactions of μ-mesons. The effectiveness of this method of discrimination against μ-bursts will be discussed later in more detail.

In what follows we shall concern ourselves with the various categories of events listed in Table I, which also contains the symbols used to describe these events. The corresponding counting rates were measured as functions of the absorber thickness above tray A and as functions of the height of the pulses from the ionization chamber. In order to take more extensive data at 10,600 feet, slight changes were made in the equipment between the sea level and the high altitude runs.

III. RESULTS

1. Summary of Experimental Data

The most significant results obtained at sea level with the experimental arrangement shown in Fig. 1(a) are summarized in Table II. Similarly, Table III contains the results obtained at 10,600 feet with the experimental arrangement shown in Fig. 1(b).[8] The counting rates shown in these tables have been corrected for accidental electronic coincidences, and also for the overlap of pen marks on the recording tape of the Esterline-Angus recorder. Both these corrections are of the order of one percent and tend to cancel since they are of opposite sign.

2. Comparison with Previous Results

The altitude variation and the absorption in lead obtained in the present measurements may be compared with previous results from similar experiments. Table IV shows the coincidence rates involving $I_{0.3}$ pulses (i.e., pulses of the ionization chamber greater than 0.3 times an α-particle pulse) observed at sea level and at 10,600 feet with Σ' alone above the chamber. A cor-

TABLE II. Summary of the most significant hourly coincidence rates obtained at sea level by means of the experimental arrangement shown in Fig. 1, with different absorbers above counter tray A. The absorber Σ' consisted of 20 g cm^{-2} of iron plus 57 g cm^{-2} of lead. The reduction of the coincidence rates caused by absorption in 455 g cm^{-2} lead is shown.

Coincidence event	$AI_{0.3}$	$AI_{0.3}B$	$AI_{0.3}BC_0$	$AI_{0.3}BC_1$	$AI_{0.3}BC_2$	$AI_{0.6}$	$AI_{0.6}B$	$AI_{1.1}$
(a) Σ' on $\Sigma=0$ g cm^{-2}	2.19±0.06	1.82±0.05	0.99±0.04	0.53±0.03	0.30 ±0.02	0.61±0.03	0.52±0.03	0.21±0.02
(b) Σ' on $\Sigma=455$ g cm^{-2} Pb	1.38±0.04	1.21±0.03	0.70±0.03	0.38±0.02	0.135±0.01	0.39±0.03	0.36±0.02	0.15±0.01
Ratio of (b) to (a)	0.64±0.02	0.67±0.02	0.78±0.04	0.72±0.06	0.45 ±0.04	0.65±0.04	0.69±0.06	0.72±0.08

[8] As indicated above, the two experimental arrangements were identical except for the method of stacking the lead in the absorber Σ and the slightly different pressures in the ionization chambers.

TABLE III. Summary of the most significant hourly coincidence rates obtained at 10,600 feet by means of the experimental arrangement shown in Fig. 1, with different absorbers above counter tray A. The absorber Σ' consisted of 20 g cm^{-2} of iron plus 57 g cm^{-2} of lead.

Absorber	Ion chamber pulse size	AIB	A_1IB	$AIBC_0$	A_1IBC_0	$AIBC_1$	A_1IBC_1	$AIBC_2$	A_1IBC_2
Σ' off									
Σ 0 g cm^{-2}	$I_{0.3}$	12.25 ±0.45	9.92 ±0.40	6.80 ±0.33	6.00 ±0.30	2.37 ±0.19	2.05 ±0.18	3.08 ±0.21	1.90 ±0.17
	$I_{0.6}$	4.62 ±0.26	3.17 ±0.21	2.40 ±0.19	2.11 ±0.18	0.77 ±0.11	0.68 ±0.10	1.63 ±0.16	0.88 ±0.12
	$I_{0.9}$	2.74 ±0.21	2.10 ±0.18	1.32 ±0.14	1.22 ±0.14	0.32 ±0.07	0.27 ±0.06	1.11 ±0.13	0.61 ±0.10
	$I_{1.2}$	1.72 ±0.16	1.31 ±0.14	0.80 ±0.11	0.74 ±0.11	0.20 ±0.06	0.15 ±0.05	0.72 ±0.10	0.41 ±0.08
Σ' on									
Σ 0 g cm^{-2}	$I_{0.3}$	12.75 ±0.23	7.80 ±0.18	6.27 ±0.16	4.57 ±0.14	2.60 ±0.10	1.64 ±0.08	3.88 ±0.12	1.59 ±0.08
	$I_{0.6}$	4.93 ±0.15	2.85 ±0.12	2.15 ±0.10	1.53 ±0.08	0.809 ±0.059	0.544 ±0.049	1.96 ±0.09	0.774 ±0.058
	$I_{0.9}$	2.93 ±0.11	1.59 ±0.08	1.17 ±0.07	0.832 ±0.058	0.480 ±0.044	0.31 ±0.04	1.26 ±0.07	0.450 ±0.042
	$I_{1.2}$	1.91 ±0.09	0.977 ±0.063	0.702 ±0.053	0.507 ±0.045	0.28 ±0.03	0.16 ±0.03	0.930 ±0.06	0.31 ±0.04
Σ' on									
Σ =114 g cm^{-2} Pb	$I_{0.3}$	10.05 ±0.23	5.24 ±0.17	4.61 ±0.15	2.92 ±0.12	2.20 ±0.11	1.31 ±0.08	3.24 ±0.13	1.01 ±0.07
	$I_{0.6}$	3.82 ±0.15	1.84 ±0.10	1.48 ±0.09	0.92 ±0.07	0.73 ±0.07	0.46 ±0.05	1.61 ±0.10	0.47 ±0.05
	$I_{0.9}$	2.21 ±0.11	1.02 ±0.08	0.90 ±0.07	0.55 ±0.06	0.33 ±0.04	0.21 ±0.04	0.99 ±0.08	0.28 ±0.04
	$I_{1.2}$	1.39 ±0.09	0.62 ±0.06	0.50 ±0.05	0.30 ±0.04	0.19 ±0.03	0.12 ±0.03	0.69 ±0.06	0.21 ±0.04
Σ' on									
Σ =341 g cm^{-2} Pb	$I_{0.3}$	5.28 ±0.15	2.51 ±0.11	2.15 ±0.10	1.36 ±0.08	1.21 ±0.07	0.687 ±0.054	1.93 ±0.09	0.467 ±0.044
	$I_{0.6}$	2.16 ±0.10	0.932 ±0.061	0.787 ±0.058	0.452 ±0.044	0.42 ±0.04	0.24 ±0.03	0.963 ±0.064	0.24 ±0.03
	$I_{0.9}$	1.24 ±0.07	0.523 ±0.047	0.41 ±0.04	0.23 ±0.03	0.22 ±0.03	0.13 ±0.02	0.613 ±0.051	0.16 ±0.03
	$I_{1.2}$	0.809 ±0.058	0.37 ±0.04	0.26 ±0.03	0.15 ±0.03	0.15 ±0.03	0.088 ±0.020	0.40 ±0.04	0.12 ±0.02

rection factor taking into account the different response of the chambers used at the two elevations was applied to the sea level rates. Table IV also shows the absorption thickness in air for the different events, computed under the assumption of exponential absorption between 10,600 feet (710 g cm^{-2} atmospheric depth) and sea level. The absorption thickness in air for the event $AI_{0.3}BC_2$ (see Table I) is 119±5 g cm^{-2}, in good agreement with the values found at airplane altitudes for charged particles producing ionization bursts of similar magnitude under thick lead shields.[4,5] Our results are also in good agreement with the results of Tinlot[9] and of Walsh and Piccioni[10] on the altitude variation of penetrating showers. Our instrument selects nearly vertical rays, and thus the values of the absorption thickness refer to approximately vertical incidence.

There is evidence that the absorption thickness in air decreases when events associated with larger ionization bursts are considered. This point will be discussed in Sec. III.6.

Table II shows that at sea level the rate of event $AI_{0.3}BC_2$ is decreased in the ratio of 1 to 0.45±0.04 when Σ is increased from 0 to 445 g cm^{-2} of lead. From Table III one computes a decrease in the ratio of 1 to 0.50±0.03 for the same event in an absorber thickness of 341 g cm^{-2} of lead at 10,600 feet. If for comparison purposes one assumes exponential absorption in Σ, one finds an absorption thickness of 550±70 g cm^{-2} of lead at sea level and an absorption thickness of 490±40 g cm^{-2} of lead at 10,600 feet. These values may be compared with the result of a similar measurement by Bridge and Rossi[4] at 14,300 feet; they obtained 430±90 g cm^{-2} as the absorption thickness in lead. As will be apparent later, the agreement is partly fortuitous.

[9] J. H. Tinlot, Phys. Rev. **74**, 1197 (1948).
[10] T. G. Walsh and O. Piccioni, Phys. Rev. **80**, 619 (1950).

3. Separation of Electromagnetic and Nuclear Interactions

As previously stated, ionization bursts can be caused either by nuclear interactions of N-rays or by electromagnetic interactions of μ-mesons. Table II shows that at sea level the addition of the absorber Σ reduces the rate of the $AI_{0.3}BC_2$ events more strongly than the rate of the $AI_{0.3}BC_0$ or $AI_{0.3}BC_1$ events. Similarly, Table IV shows that 320 g cm^{-2} of atmosphere reduces the rate of the $AI_{0.3}BC_2$ events much more strongly than the rate of the $AI_{0.3}BC_0$ or $AI_{0.3}BC_1$ events. These results together with the well-known difference in penetrating power of N-rays and μ-mesons prove that the requirement of a multiple discharge in tray C discriminates effectively in favor of nuclear interactions as had been anticipated. Indeed, a μ-meson can produce an $AIBC_2$ coincidence only through two successive electromagnetic interactions, one occurring above the ionization chamber and one in the lead between the ionization chamber and tray C. This is necessary because for the energies involved in this experiment, an electronic shower starting above the ionization chamber has virtually zero probability of penetrating the lead block below the chamber. One can easily show that the contribution of such double interactions to the recorded $AIBC_2$ rate is small. It is known that

TABLE IV. Comparison of the coincidence rates obtained at sea level and at 10,600 feet with only absorber Σ' present. (a) The sea level coincidence rates in counts per hour multiplied by 0.86±0.08 to normalize to the chamber used at 10,600 feet. (b) The increase in the coincidence rates from sea level to 10,600 feet (710 g cm^{-2}). (c) The absorption thickness in g cm^{-2} of air computed under the assumption that the absorption is exponential.

	$AI_{0.3}B$	$AI_{0.3}BC_0$	$AI_{0.3}BC_1$	$AI_{0.3}BC_2$
(a) counts/hour	1.56±0.15	0.85±0.09	0.45±0.05	0.26±0.03
(b) factor increase	8.16±0.80	7.39±0.79	5.76±0.67	14.9±1.8
(c) absorption thickness g cm^{-2} of air	153±7	160±9	183±19	119±5

TABLE V. Separation of μ-meson and N-component induced coincidence events for absorber Σ' alone above the detector. Coincidence rates are in counts per hour. The standard errors listed have been calculated under the assumptions that the calculated μ-meson altitude variation has no statistical error and the altitude variation of the N-component is of the same statistical accuracy as the altitude variation of the $AI_{0.3}BC_2$ events.

	$AI_{0.3}B$		$AI_{0.3}BC_0$		$AI_{0.3}BC_1$	
	N-comp.	Mu-meson	N-comp.	Mu-meson	N-comp.	Mu-meson
Sea level	0.79±0.09	0.77±0.11	0.38±0.05	0.47±0.07	0.15±0.03	0.30±0.05
10,600 ft	11.83±0.28	0.92±0.13	5.71±0.19	0.56±0.08	2.24±0.12	0.36±0.06

out of 100 cosmic-ray μ-mesons emerging from a lead block only about 7 are accompanied by an electron.[11,12] If one makes the extreme assumption that all $AIBC_1$ events are caused by μ-mesons, the number of $AIBC_2$ events due to μ-mesons can only be 7 percent of the number of $AIBC_1$ events. This figure may be compared with the experimental results at sea level: with $\Sigma=0$ the ratio of the $AI_{0.3}BC_2$ rate to the $AI_{0.3}BC_1$ rate is 0.57±0.05, and with $\Sigma=455$ g cm^{-2} of lead the ratio is still 0.35±0.03.

Underground experiments substantiate the view that at sea level and above, the N-rays rather than the μ-mesons are responsible for events capable of discharging two heavily shielded Geiger counters in coincidence with an ionization chamber.[13,14] This view is also supported by our finding that the absorption in lead of the radiation responsible for $AIBC_2$ events is approximately the same at 10,600 feet as at sea level. The absorption in lead of the radiation responsible for $AIBC_0$ and $AIBC_1$ events, on the other hand, increases with decreasing atmospheric depth, which shows that at sea level a large part of this radiation consists of μ-mesons.

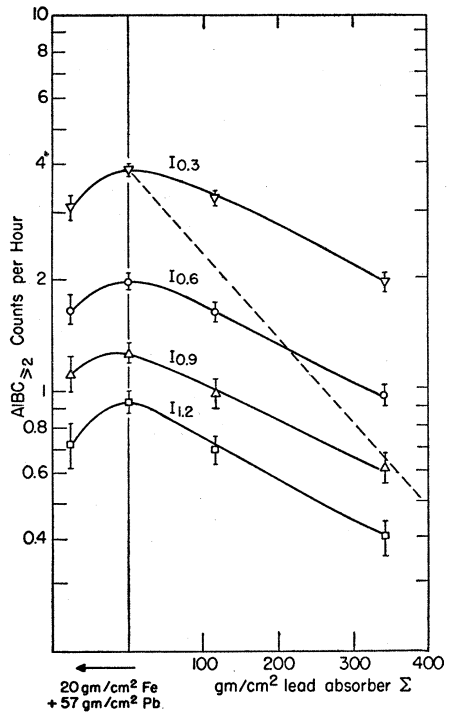

FIG. 3. The coincidence rate $AIBC_2$ at 10,600 feet as a function of the absorber thickness above the detector for four different values of the minimum detected ionization chamber pulse. The 20 g cm^{-2} of iron and 57 g cm^{-2} of lead compose the absorber Σ'. The dashed line shows an exponential absorption $\exp(-x/L)$ with $L=195$ g cm^{-2}.

It is important to evaluate quantitatively the contributions of N-rays and μ-mesons to the $AI_{0.3}BC_0$ and $AI_{0.3}BC_1$ rates recorded at sea level and at 10,600 feet. For this evaluation we computed that the number of $AI_{0.3}BC_0$ and $AI_{0.3}BC_1$ events produced by μ-mesons increases in the ratio 1 to 1.20 between sea level and 10,600 feet.[7] Further, we assumed that the number of $AI_{0.3}BC_0$ or $AI_{0.3}BC_1$ events produced by the N-component increases between these two altitudes in the same ratio as the number of $AI_{0.3}BC_2$ events. From the observed altitude variation in the $AI_{0.3}BC_0$ and $AI_{0.3}BC_1$ rates we then found, with a simple calculation, the results summarized in Table V, which are for absorbers Σ' on and $\Sigma=0$ g cm^{-2}. One sees from the table that at 10,600 feet (91±1) percent of the $AI_{0.3}BC_0$ events and (86±2) percent of the $AI_{0.3}BC_1$ events are due to nuclear interactions, while at sea level (45±5) percent of the $AI_{0.3}BC_0$ events and (33±5) of the $AI_{0.3}BC_1$ events are due to nuclear interactions. For the $AI_{0.3}B$ events at 10,600 feet (92±1) percent of the coincidence rate is due to nuclear interactions, while at sea level (51±5) percent of the coincidence rate is due to nuclear interactions.

4. Absorption of the N-Component in Lead

Figure 3 shows logarithmic plots of the coincidence rates as a function of absorber thickness for the $AIBC_2$ events obtained at 10,600 feet. The various curves correspond to different values of the minimum size of the ionization burst.

From our own results and from those of other experimenters it is known that the absorption curve in air of the N-component of cosmic rays is practically exponential with an absorption thickness close to 120 g cm^{-2}. If one assumes that air and lead absorbers differ only because of the change in nuclear radius, one would also expect an approximately exponential absorption of the N-radiation in lead. From the model of the semi-transparent nucleus[15] and from the experimental value

[11] W. E. Hazen, Phys. Rev. **64**, 7 (1943).
[12] Brown, McKay, and Palmatier, Phys. Rev. **76**, 506 (1949).
[13] E. P. George and A. C. Jason, Nature **160**, 327 (1947).
[14] D. E. Hudson, thesis, Cornell University (1950).
[15] Fernbach, Serber, and Taylor, Phys. Rev. **75**, 1352 (1949).

of the absorption thickness in air, one computes an absorption thickness of 195 g cm^{-2} in lead.[16]

Figure 3 shows the observed absorption in lead for the $AIBC_2$ events compared to the result of the above computation. It is evident that the absorption is much smaller than that predicted. Indeed, the absorption curves are not exponential, but exhibit "transition effects"; the rate of events increases slightly at first with increasing absorber thickness and then decreases again. It thus seems necessary to conclude that the difference in density between the air and lead absorbers has an important effect on the observed absorption curves.

The most likely explanation for this effect is that π-mesons produced in high energy nuclear interactions can give rise to further nuclear interactions capable of producing the observed coincidences. In air, most π-mesons will decay before colliding with nuclei. In lead, instead, most π-mesons will interact before decaying. Thus the total number of interacting particles (nucleons and π-mesons) is greater under an air plus lead absorber than under an equivalent thickness of air alone.

In 1948, when the present experiment was initiated, very little was known about the nuclear interactions of π-mesons. Today, from the work with artificially produced π-mesons, it is known that π-mesons with energies of the order of 100 Mev interact strongly with nuclei,[17] and observations by means of cloud chambers and photographic plates have shown that the same is true for the π-mesons of higher energy which occur in the nuclear interactions of cosmic rays.[18–21] In agreement with these results, the present experiment shows that π-mesons of several Bev such as are necessary to

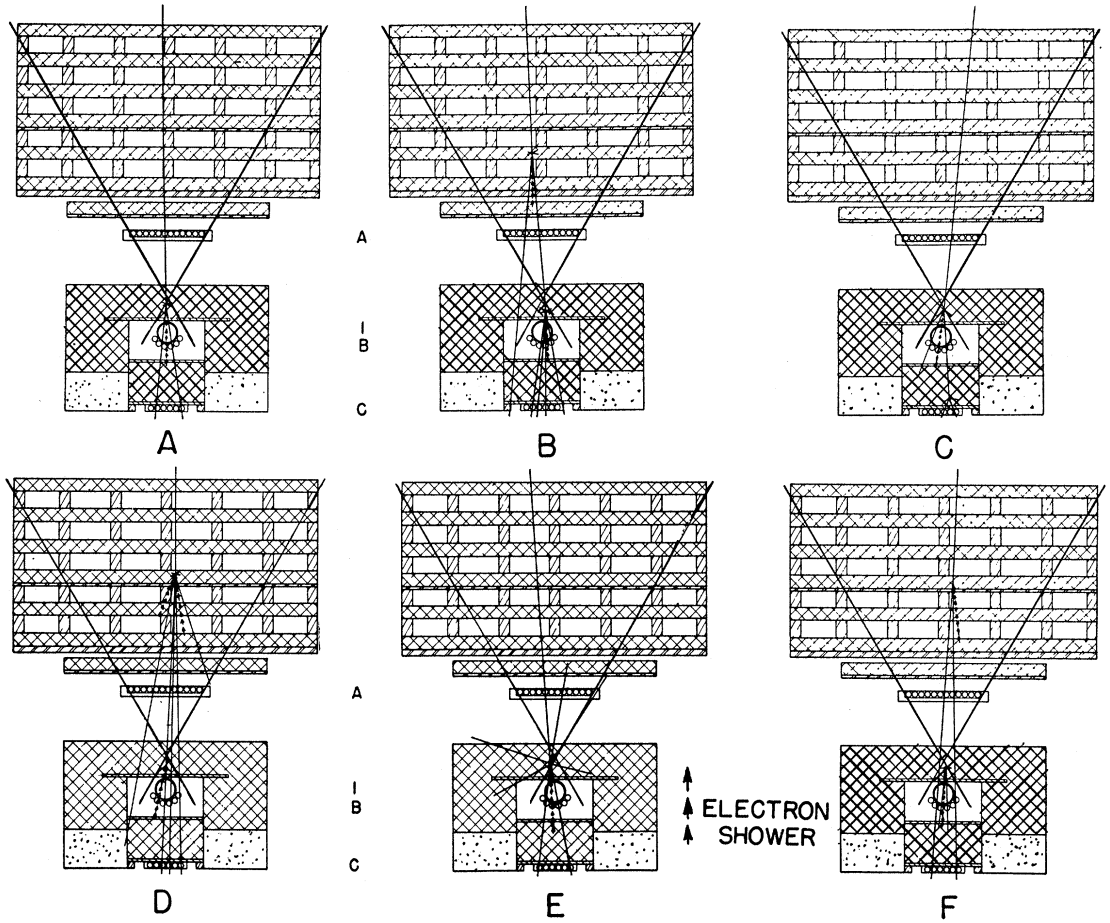

FIG. 4. Schematic representation of six different cosmic-ray processes capable of producing the $AIBC_2$ coincidence events.

[16] This conclusion is not invalidated by the fact that in air there is some reproduction of the N-radiation. For a discussion of this point and for a more detailed description of the method used to determine the collision mean free path in Sec. III.5 see Bruno Rossi, *High Energy Particles* (Prentice-Hall, Inc., New York, 1952), Chap. VIII.

[17] See, for example, Bernardini, Booth, and Lederman, Phys. Rev. **83**, 1075 (1951).

[18] B. P. Gregory and J. H. Tinlot, Phys. Rev. **81**, 675 (1951).

[19] A. J. Hartzler, Phys. Rev. **82**, 359 (1951).

[20] Camerini, Fowler, Lock, and Muirhead, Phil. Mag. **41**, 413 (1950).

[21] M. Annis, thesis, Massachusetts Institute of Technology (1951).

produce the recorded events possess large cross sections for nuclear interactions.

Before accepting this conclusion two other possible explanations of the "transition effect" will be considered. First there is the possibility that the model of the semitransparent nucleus is oversimplified in that the nucleons of a complex nucleus do not act independently of one another in high energy collisions. In this case, a "transition effect" could occur in passing from air to lead. The most convincing evidence that the observed initial increase in the counting rate does not depend on the atomic number but on the density comes from the results obtained with a carbon absorber for Σ.[22] Exactly the same type of absorption curve was obtained in this case as in the experiment here reported.

The second effect considered is the "geometric coherence" of particles produced in Σ. A nuclear interaction that takes place in the absorber may produce two or more secondary particles which then produce the observed coincidence only because of their striking the detecting equipment simultaneously. If the same interaction occurred in air, the secondary particles would in most cases be so widely separated at the detector that no such coincidence would be possible.

Figure 4 shows schematically six different possible causes for events $AIBC_2$. The coincidences recorded in cases D and F are due to geometrical coherence. In both these cases a nuclear interaction occurs in the absorber Σ. In case D, one of the secondary charged particles from this interaction discharges a counter in tray A and then interacts in the lead producing layer above the ionization chamber to cause a burst in the chamber and discharge tray B. The coincidence that results from this secondary particle is A_1IBC_0 (only one counter discharged in tray A and no counter discharged in tray C). Other secondary particles, from the nuclear interaction in Σ, discharge counters in trays A, B, and C, and the detected coincidence shows more than one counter discharged in tray A and more than one counter discharged in tray C. In case F one of the secondary neutrons from the interaction in the absorber interacts in the lead above the ionization chamber causing an ionization burst and discharging a counter in tray B. This event would not be recorded, but associated charged secondaries from the nuclear interaction in Σ discharge counters in trays A and C, and an $AIBC_2$ coincidence is detected.

One may mention another possible coherence effect, which is not illustrated in Fig. 4. In a nucleonic cascade initiated in the lead absorber and propagating through the absorber and the producing layer, the secondary particles remain concentrated in a fairly small region around the trajectory of the initiating particle. Such a cascade may have a sufficient density of ionizing particles at the ionization chamber to produce a detectable burst, while this may not be the case for similar cascades initiated in air.

In order to obtain some information regarding the coherence effects we performed an additional experiment at 10,600 feet; 114 g cm^{-2} of lead were placed, first directly below tray A, then directly above tray A, then 66 cm above tray A, and then were completely removed. All other experimental conditions including the solid angle subtended by the absorber at the detector were kept constant.[23]

When the 114 g cm^{-2} lead shield was directly above tray A, geometric coherence between secondary particles from nuclear interactions in this shield should have been most effective in producing detected events. When the 114 g cm^{-2} lead shield was 66 cm above tray A, many of the events due to geometric coherence should have been missed. (Note, however, that the solid angle presented by tray C to secondary particles produced in interactions 66 cm above tray A is of the order of 0.04 steradian and may not be small enough to eliminate all coherence effects.) When the 114 g cm^{-2} lead shield was below tray A, neutrons incident on this shield could not produce detected events (neglecting back emission). In this case, events caused by associated secondary particles from neutron induced interactions in the 114 g cm^{-2} shield were not detected. These events would be detected with the 114 g cm^{-2} lead shield directly above tray A; they would not be detected in measurements of atmospheric absorption. A change in the coincidence rates when the 114 g cm^{-2} shield was moved from directly above to directly below tray A could also be caused by a change in the relative number of protons and neutrons as the radiation passes from air to lead.

The results of the coherence experiment are given in Table VI. One sees that the rate of the $AI_{0.3}BC$ events does not depend, within the statistics, on the position of the 114 g cm^{-2} absorber. In Fig. 5 we have plotted the absorption data for the $AI_{0.3}BC$ rates given previously in Table III as well as that from the coherence experiment given in Table VI.[24] The dashed line repre-

TABLE VI. The hourly coincidence rates for the events $AI_{0.3}BC$ at 10,600 feet with 114 g cm^{-2} of lead in different positions with respect to the detector. The experimental arrangement was the same as that of Fig. 1 with both Σ and Σ' removed, except that 171 g cm^{-2} instead of 142 g cm^{-2} of lead was kept permanently between the ionization chamber and tray A. The results shown in this table have been corrected for fluctuations in barometric pressure.

114 g cm^{-2} Pb removed	114 g cm^{-2} Pb directly above tray A	114 g cm^{-2} Pb directly below tray A	114 g cm^{-2} Pb 66 cm above tray A
6.28±0.19	6.08±0.23	5.63±0.21	5.94±0.22

[22] R. Rediker, unpublished results. Measurements for carbon and hydrocarbon absorbers will be reported in a subsequent communication.

[23] For all the coherence experiments absorbers Σ and Σ' were removed and an additional 29 g cm^{-2} of lead was added between tray A and the ionization chamber.

[24] The absorption points obtained from the coherence experiment with the 114 g cm^{-2} of lead removed and with the 114 g cm^{-2} of lead directly above tray A fit the absorption curve

sents the expected result computed from the absorption in air as discussed above. The impossibility of explaining solely in terms of a coherence effect, the discrepancy between the observed absorption in lead and that expected from the absorption in air is evident from the figure. The counting rate for the $AI_{0.3}BC$ events with the 114 g cm^{-2} absorber directly above tray A is about 2.2 counts per hour greater than the calculated value, and placing the 114 g cm^{-2} absorber either 66 cm above the tray or directly underneath it, does not change this figure significantly.

Use of the $AI_{0.3}BC$ events rather than $AI_{0.3}BC_2$ events in determining the results of the coherence experiment is justified because the absorption curve for the $AI_{0.3}BC$ events exhibits the same type of "transition effect" as the absorption curves for the $AIBC_2$ events (see Figs. 3 and 5).

We have corrected the results of the coherence experiment for fluctuations in the barometric pressure using an absorption thickness in air for the producing radiation of 119 g cm^{-2}. These are the only results reported in this paper that are corrected for pressure fluctuations. We did not correct the results shown in Table VI and Fig. 5 for μ-bursts because we did not wish to introduce into the comparison of the counting rates the additional statistical errors inherent in making the μ-meson correction. Mu-bursts, which account for only about ten percent of the $AI_{0.3}BC$ coincidence rate, have been included in computing the expected absorption indicated by the dashed line in Fig. 5. The effect of the μ-meson induced events on the barometric correction has been neglected.

There is thus little doubt that π-mesons are mainly, if not totally, responsible for the difference between the absorption curve in lead observed directly and that computed from the experimental absorption curve in air on the basis of the model of the semitransparent nucleus.

Unfortunately, it is not possible to discuss the absorption curves quantitatively. The experimental errors are fairly large, the coherence effects may not be completely negligible, and the "zero thickness" for the lead absorber is somewhat undetermined, for it depends on the position in the lead above the chamber where the detected nuclear interactions occur. It is possible, however, to make some qualitative statements.

(a) If the initial increase in the absorption curves is not entirely due to spurious effects, but represents a real increase in the number of burst producing particles, the average energy of the interacting particles (nucleons and π-mesons) must decrease in passing from air to lead. Obviously the total energy of the particles cannot increase. The decrease in average energy means either that the energy spectrum becomes steeper (i.e., the relative number of lower energy particles is greater in lead than in air) or that the minimum energy necessary to produce a detectable interaction is smaller for π-mesons than for nucleons. It is conceivable that there is a different distribution of available energy between secondary nucleons and π-mesons in the nuclear interactions of the two kinds of particles.

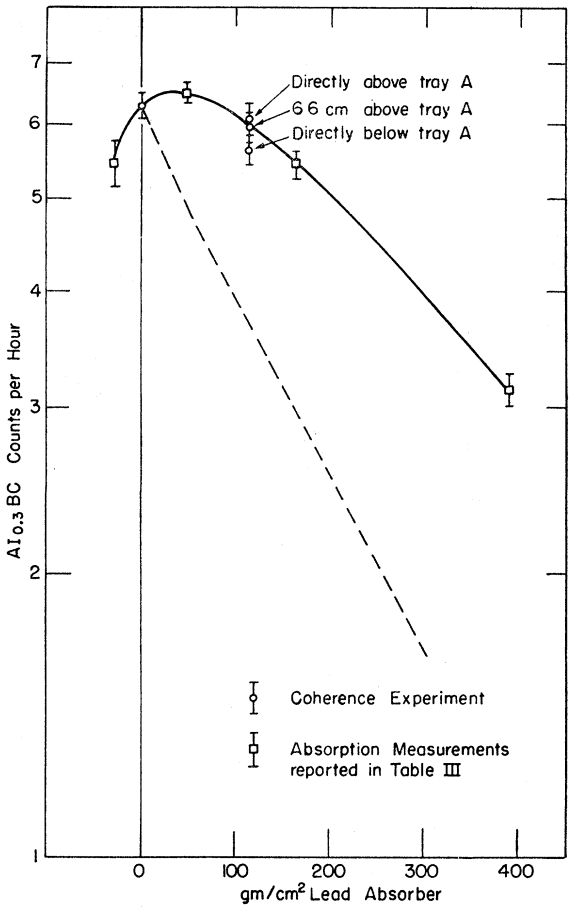

FIG. 5. The results of the "coherence experiment" at 10,600 feet. The rate of $AI_{0.3}BC$ events as a function of absorber thickness as determined from the results given in Table III (assuming the 20 g cm^{-2} of iron equivalent to 20 g cm^{-2} of lead) has been superimposed. The dashed line shows the absorption that would be expected for the $AI_{0.3}BC$ events from the model of the semitransparent nucleus and from the experimental value of the absorption thickness in air.

(b) It is reasonable to assume that after a sufficient thickness of lead, a condition of approximate equilibrium between π-mesons and nucleons will be reached. The absorption curves will then become nearly exponential and the experimental value of the absorption thickness will represent an upper limit for the collision mean free path of all interacting particles. The thickness of lead at which the approximate equilibrium is reached may be much larger than that used in the present experiment. However, the experimental absorption thickness will still give an upper limit (possibly a very high limit) for the collision mean free path of all interacting particles. From Fig. 3, one finds that the absorption at large values of the absorber Σ corresponds to absorption thicknesses of 440±50 g cm^{-2} for the $AI_{0.3}BC_2$ events and 420±100 g cm^{-2} for the $AI_{1.2}BC_2$ events. Thus the collision mean free path for high

(Fig. 5) very well. Since the coherence experiment was performed one year after the experiment reported in this paper, the excellent fit of these points is additional evidence for the reliability of our experimental results.

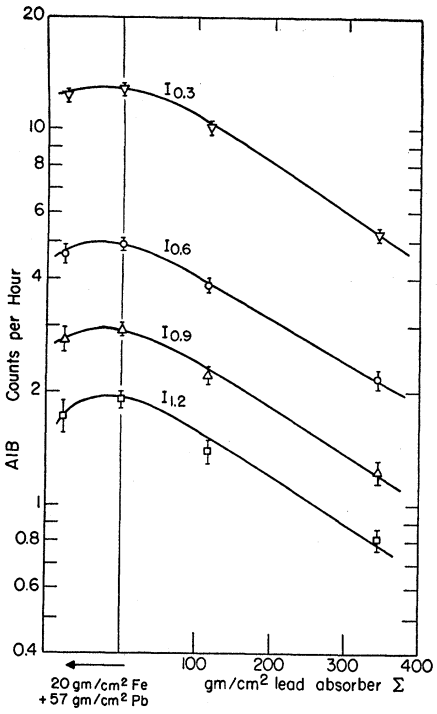

FIG. 6. The coincidence rate AIB at 10,600 feet as a function of the absorber thickness above the detector for four different values of the minimum detected ionization chamber pulse. The 20 g cm^{-2} of iron and the 57 g cm^{-2} of lead compose the absorber Σ'. The coincidence rates have not been corrected for μ-meson induced bursts.

energy π-mesons which produce these events must be smaller than these values.

(c) The "transition effects" in the absorption curves for lead explain the large values of the absorption thickness that have previously been reported from similar ionization chamber experiments.[4,14,25]

The absorption data for events other than those discussed above ($AIBC_2$ and $AIBC$) are given in Fig. 6, Fig. 7, and Table VII. Figure 6 shows the coincidence rate AIB as a function of absorber thickness for the four different values of the minimum pulse required in the ionization chamber. These rates are not corrected for μ-bursts.

Figure 7 and Table VII give the absorption data for the $AI_{0.3}B$, $AI_{0.3}BC_0$, and $AI_{0.3}BC_1$ events corrected for μ-bursts. The μ-meson correction for absorbers Σ' on and $\Sigma=0$ was made using the results of Sec. III.3 above. For other absorbers the additional absorption of the μ-mesons was taken into account only approximately with the assumptions listed in Table VII.[26] The general features of the absorption curves shown in Figs. 6 and 7 are similar to those discussed above (see Figs. 3 and 5).

5. The Interaction Mean Free Path of the *N*-Component in Lead

In Sec. III.4 we have discussed the variation of the various coincidence rates when additional absorbers were placed above tray A. We have interpreted these variations as a direct indication of the effect of the absorber on the number of particles above tray A capable of producing the various types of coincidences.

In this section we will discuss the variation with absorber thickness of the rates of those coincidence events in which one and only one counter in tray A was struck (A_1 events). This requirement rules out many of the events in which the incident particle interacts in the absorber. If the collision in the absorber gives rise to a particle capable of interacting in the lead above the ionization chamber, it is likely that other ionizing particles are produced and that more than one counter in tray A will be discharged (see Fig. 4, cases B, D, and F). If the A_1 requirement could be used to eliminate all collisions in the absorber, the variation with absorber thickness of the rate of occurrence of A_1 events would yield directly the interaction mean free path of the particles responsible for the observed bursts.[16]

The requirement that only one counter be struck in tray A does not, of course, completely eliminate the

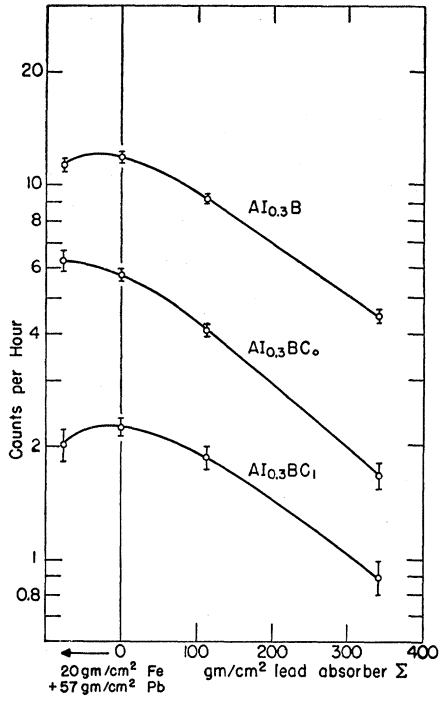

FIG. 7. The coincidence rate as a function of absorber thickness is plotted for the $AI_{0.3}B$, the $AI_{0.3}BC_0$, and for the $AI_{0.3}BC_1$ rates at 10,600 feet. The coincidence rates have been corrected for μ-meson induced bursts. The assumptions listed in Table VII were used to determine the absorption in lead of the burst-producing μ-mesons.

[25] T. G. Stinchcomb, Phys. Rev. **83**, 422 (1951).

[26] A better computation of this absorption similar to that described in the appendix was not performed because the effect of an inaccuracy in the μ-meson absorption on the computation of the N-component rates is small.

TABLE VII. The absorption of the separated N-component that produces different coincidence events at 10,600 feet. The coincidence rates are in counts per hour. We have assumed that in all bursts produced by μ-mesons, only one counter in tray A was struck. We have calculated the absorption in lead of the μ-mesons which produce the bursts by assuming: (a) All μ-mesons of energy above 5×10^9 ev which were incident upon the detector with Σ' on and $\Sigma=0$ g cm^{-2} contributed with equal weight to producing the bursts. (b) The integral range spectrum at sea level for μ-mesons of the energies under consideration was applicable at 10,600 feet. The integral range spectrum given by B. Rossi, Revs. Modern Phys. **20**, 537 (1948), was used in conjunction with the range-energy relation for μ-mesons in lead given by G. C. Wick, Nuovo cimento **9**, 310 (1943). It should be noted when comparing rates at different absorber thicknesses that the standard errors in the rates for the separated N-component are not statistically independent.

		$AI_{0.3}B$		$AI_{0.3}BC_0$		$AI_{0.3}BC_1$	
Σ'	Σ	N-comp.	Mu-meson	N-comp.	Mu-meson	N-comp.	Mu-meson
Off	0 g cm^{-2}	11.31±0.47	0.94±0.13	6.23±0.34	0.57±0.08	2.00±0.20	0.37±0.06
On	0 g cm^{-2}	11.83±0.28	0.92±0.13	5.71±0.19	0.56±0.08	2.24±0.12	0.36±0.06
On	114 g cm^{-2}	9.16±0.27	0.89±0.13	4.07±0.17	0.54±0.08	1.85±0.13	0.35±0.06
On	341 g cm^{-2}	4.45±0.19	0.83±0.12	1.64±0.12	0.51±0.07	0.89±0.09	0.32±0.05
		$A_1I_{0.3}B$		$A_1I_{0.3}BC_0$		$A_1I_{0.3}BC_1$	
Off	0 g cm^{-2}	8.98±0.42	0.94±0.13	5.43±0.31	0.57±0.08	1.68±0.19	0.37±0.06
On	0 g cm^{-2}	6.88±0.22	0.92±0.13	4.01±0.16	0.56±0.08	1.28±0.10	0.36±0.06
On	114 g cm^{-2}	4.35±0.21	0.89±0.13	2.38±0.14	0.54±0.08	0.96±0.10	0.35±0.06
On	341 g cm^{-2}	1.68±0.16	0.83±0.12	0.85±0.10	0.51±0.07	0.37±0.07	0.32±0.05

effects of secondary particles produced in the absorber. The accompanying particles may fail to emerge from the absorber; or they may miss tray A either because they are emitted at wide angles or because they pass through the "holes" between the counters. It is also possible that two or more particles pass through the same counter in tray A. Therefore, the mean free paths deduced from the experimental absorption curves for the A_1 events will be somewhat greater than the actual collision mean free paths.

Figure 8 shows the reduction in coincidence rates with addition of absorber for the $A_1I_{0.3}$ type of coincidences corrected for μ-meson background. Table VIII shows the mean free paths computed from the results shown in Fig. 8. The values have been obtained from a least squares treatment of the data, assuming an exponential decrease of the rates with thickness. Of the events tabulated, it is seen that the $A_1I_{0.3}BC_0$ rate shows the greatest absorption. This is probably related to the fact that when events with multiple counter discharges in tray A are included, secondary particles from nuclear interactions in the absorber contribute to a lesser extent to events of the $AIBC_0$ type than to events of the $AIBC_1$ or $AIBC_2$ type, as shown by the much smaller "transition effect" exhibited by the $AIBC_0$ events compared to the other events (see Figs. 3 and 7).

In Fig. 9, the A_1IBC_0 coincidence rates uncorrected for μ-bursts are plotted as functions of the absorber thickness for different ionization chamber biases. The fact that the points at $\Sigma=341$ g cm^{-2} are high may be explained with the argument that as the absorber gets thicker, tray A becomes less efficient in detecting interactions because of the angular divergence and the absorption of secondaries. The logarithmic slopes of the uncorrected A_1IBC_0 curves increase with increasing pulse height. While the mean free path obtained for the $A_1I_{0.3}BC_0$ events corrected for μ-mesons is 225±14 g cm^{-2} (see Table VIII), Fig. 9 indicates that, with proper μ-meson correction, the absorption of A_1IBC_0 events associated with large bursts is not inconsistent with the geometrical mean free path (167 g cm^{-2} of lead).

TABLE VIII. The mean free path in g cm^{-2} of the various $A_1I_{0.3}B$ type events under the assumption that the rates that are produced by the N-component vary exponentially with absorber thickness.

Event	$A_1I_{0.3}BC_0$	$A_1I_{0.3}BC_1$	$A_1I_{0.3}BC_2$
Mean free path in g cm^{-2}	225±14	292±41	286±23

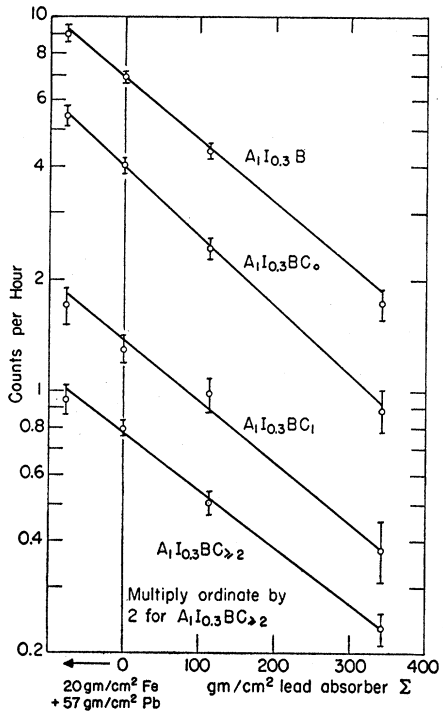

FIG. 8. The reduction of the $A_1I_{0.3}$ type of coincidence rates at 10,600 feet due to addition of absorber. The coincidence rates have been corrected for μ-meson induced bursts under the assumptions listed in Table VII.

6. Pulse-Height Distributions

Figure 10 shows double logarithmic plots of the integral pulse-height distributions observed for various events. The distributions refer to measurements taken at 10,600 feet with the absorber Σ' alone above counter tray A. The experimental results tabulated in Table III show that within the experimental errors the shape of the pulse-height distribution for a given kind of event (with the possible exception of event AIB) is independent of the thickness of absorber above tray A; it is also independent of the requirement that only one counter be discharged in tray A.

From an examination of Fig. 10 it appears that power laws of the type $N(p)=\text{constant}\times p^{-\gamma}$ represent well the integral pulse-height distributions: for the AIB events, $\gamma=1.35$; for the $AIBC_0$ events, $\gamma=1.52$; and for the $AIBC_2$ events, $\gamma=1.02$. The pulse-height distribution for the $AIBC_1$ events seems to exhibit small deviations from a power law with $\gamma=1.60$. Since the AIB events are merely the sum of the $AIBC_0$, $AIBC_1$, and $AIBC_2$ events, and the sum of three different power laws cannot give a fourth different power law, it appears that the power law assumption is a simplification which is justified only by the crudeness of the experimental data. The subtraction of the ionization bursts due to μ-mesons does not significantly change the above data.[27] Figure 10 shows that the percentage of events associated with multiple counter discharges in tray C increases with the size of the ionization pulse

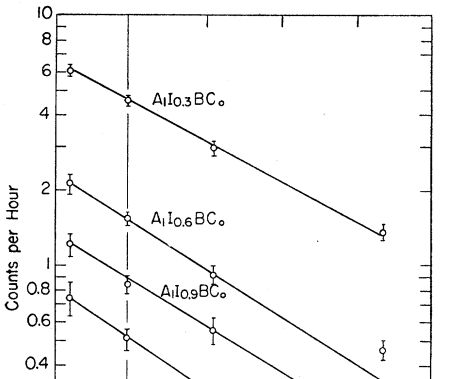

FIG. 9. The reduction of the A_1IBC_0 coincidence rates at 10,600 feet which results from addition of absorber. Data for the four values of the minimum detected ionization chamber pulse are given. The coincidence rates are not corrected for μ-meson induced bursts.

[27] To make this subtraction we used the results listed in Table V for the μ-bursts in conjunction with an integral pulse-height distribution with $N(E)=kE^{-1.6}$ (see appendix).

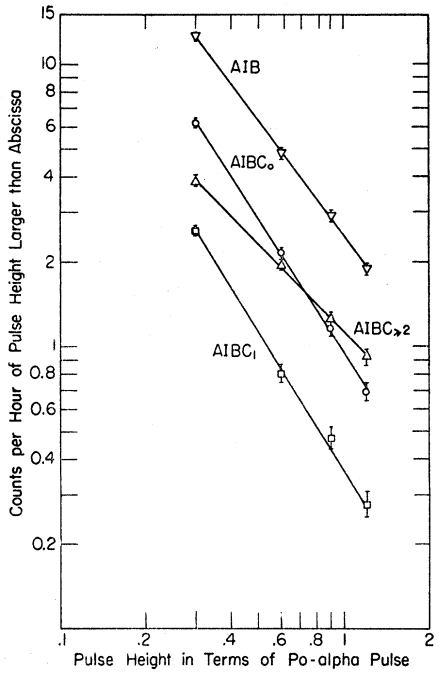

FIG. 10. The integral ionization chamber pulse-height distribution at 10,600 feet for various coincidence events. Only absorber Σ' is present.

required.[28] (30 ± 1) percent of the $AI_{0.3}B$ events and (49 ± 4) percent of the $AI_{1.2}B$ events are associated with multiple counter discharges in tray C.

The dissimilarity of the integral pulse-height distributions for the $AIBC_0$ and $AIBC_1$ events on the one hand and for the $AIBC_2$ events on the other hand shows that these coincidences are not caused by interactions of the same kind where by chance different numbers of particles strike tray C.

On the basis of the projected zenith angular distribution of penetrating particles from nuclear interactions determined by Brown and McKay,[29] one can estimate that at least 67 percent of the penetrating secondaries from recorded interactions miss tray C. This estimate can only be correct as to the order of magnitude because the angular distribution given by Brown and McKay is an average over many interactions whereas the directions of emission of secondaries from a single interaction are certainly interdependent. It is apparent, however, that most of the $AIBC_2$ events are caused by nuclear interactions in which large numbers of penetrating particles are produced. Most of the $AIBC_0$ and $AIBC_1$ events, instead, are caused by nuclear interactions in which fewer penetrating particles are produced and by interactions of μ-mesons.

Figure 11 shows double logarithmic plots of the pulse-height distributions for the AI, $AIBC_1$, and $AIBC_2$ coincidence events observed at sea level with

[28] A similar result has been reported by E. P. George and P. T. Trent, Proc. Phys. Soc. (London) **64**, 733 (1951).

[29] W. W. Brown and A. S. McKay, Phys. Rev. **77**, 342 (1950).

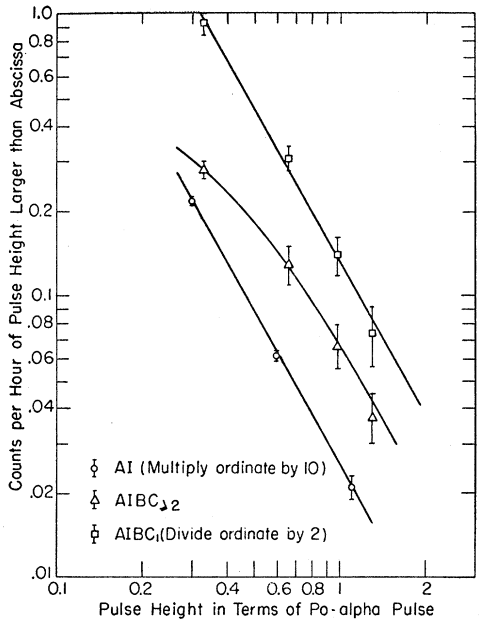

FIG. 11. The integral ionization chamber pulse-height distribution at sea level for various coincidence events. Only absorber Σ' is present.

absorber Σ' alone. It should be noted that the curves obtained with an additional absorber Σ of 455 g cm^{-2} of lead are similar to those shown in Fig. 11. The AI events and the $AIBC_1$ events are distributed according to a power law with $\gamma \approx 1.8$. The pulse-height distribution for the $AIBC_2$ coincidence events, however, shows a definite deviation from a power law, being flatter at small burst size than at large burst size. A similar deviation was also observed in the curve obtained with $\Sigma = 455$ g cm^{-2}. In Fig. 12 the pulse-height distribution for the $AIBC_2$ events at sea level is compared with the pulse-height distribution for the same events at 10,600 feet. The absolute values of the sea level rates are corrected to account for the slightly greater sensitivity of the chamber used at this location. One sees that the atmospheric absorption is stronger for the larger bursts. Under the assumption of an exponential absorption, one finds an absorption thickness in the atmosphere of 119 ± 5 g cm^{-2} for $I_{0.3}$ bursts and of 100 ± 7 g cm^{-2} for $I_{1.2}$ bursts.

An analysis of the AIB pulse-height distributions at sea level and at 10,600 feet also indicates that the atmospheric absorption of the N-component is greater for larger bursts. The observed AIB pulse-height distributions can be represented by power laws with $\gamma = 1.8$ at sea level and $\gamma = 1.4$ at 10,600 feet. In the evaluation of the fractional number of μ-bursts at the two elevations, we have used a computed value of 1.2 for increase factor in the rate of these bursts between sea level and 10,600 feet (see Sec. III.3). The calculation, given in the appendix, from which we obtain the above increase factor also indicates (see Table IX) that the pulse-height distribution of μ-bursts obeys a power law with $\gamma \approx 1.6$ both at 10,600 feet and at sea level. From these results it follows that the observed change in the AIB pulse-height distribution from 10,600 feet to sea level cannot be explained in terms of a change in the proportion of bursts induced by μ-mesons and by N-rays, respectively, unless one also assumes that the pulse-height distribution of the N-bursts becomes steeper at the lower elevation. Such a change in pulse-height distribution is explained by the increased atmospheric absorption of the N-component which produces the larger bursts.

7. Back Emission of Penetrating Particles

The histogram in Fig. 13 shows the number of cases in which either one, or more than one, counter was discharged in tray A for the $AI_{0.3}BC_0$, $AI_{0.3}BC_1$, and $AI_{0.3}BC_2$ events observed at 10,600 feet under different absorber thicknesses. For all absorber thicknesses there is a clear correlation between multiple discharges in tray A and multiple discharges in tray C. The probability for multiple discharges in tray A was least when no counter in tray C was struck. This probability increased slightly when one counter in tray C was struck, and it increased by a large amount when two or more counters in tray C were struck. Even without any lead absorber above tray A, in which case the only solid material above this tray was a canvas tent, in 38 percent of the $AI_{0.3}BC_2$ coincidences more than one counter in tray A was struck, and in 12 percent of the $AI_{0.3}BC_0$ coincidences more than one counter in

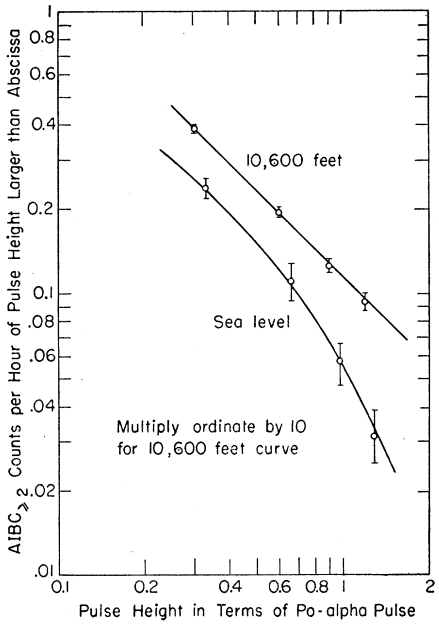

FIG. 12. The integral ionization chamber pulse-height distribution for the $AIBC_2$ coincidence event at sea level and at 10,600 feet. Only absorber Σ' is present. The sea level rates have been normalized to the ionization chamber used at 10,600 feet.

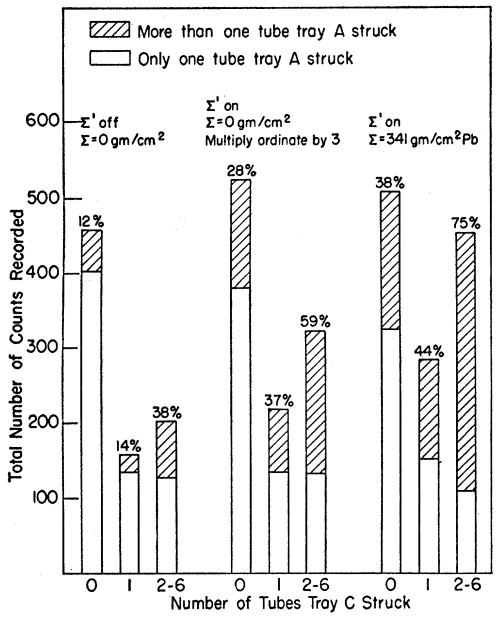

FIG. 13. Histogram showing the number of events in which more than one counter in tray A was discharged as a function of the number of counters in tray C discharged, for the $AI_{0.3}B$ coincidences at 10,600 feet with different absorbers above the detector. The percentages shown are the percentages of coincidence events in which more than one counter in tray A were struck.

tray A was struck. These results show definitely that nuclear interactions giving rise to many penetrating particles often project some of these in the backward direction. If the nuclear interaction occurred 48 g cm^{-2} of lead above the ionization chamber, a charged particle emitted directly upward with kinetic energy sufficient to reach tray A would need a minimum energy of 0.28 Bev if a proton, and 0.15 Bev if a π-meson.

From the angular distribution of penetrating particles produced in nuclear interactions as observed in cloud chambers[29] and in nuclear emulsions,[30,31] between 5 and 10 percent of the total number of penetrating particles produced would be expected to strike the A tray. It is difficult to determine whether or not this is consistent with our results, especially because as pointed out above, the results from cloud chambers and emulsions are averages over many interactions.

The possibility that some of the events are caused by backscattered photons or neutrons cannot be excluded. We performed an auxiliary experiment in which an additional 25 radiation lengths of lead were added between tray A and the ionization chamber to absorb any photons. The correlation between multiple discharges in tray A and tray C was unchanged. However, the result is ambiguous because the additional lead acts as a producer as well as an absorber of photons. It is very difficult to estimate the possible effect of the neutrons that are known to be emitted backwards in large numbers.[32]

An investigation of multiple discharges in tray A as a function of the ionization chamber pulse height showed no significant correlation between back emission of penetrating particles and burst size. It should be remembered, however, that the maximum ratio of pulse heights investigated was one to four.

IV. POSSIBLE EFFECTS OF AIR SHOWERS AND PRESSURE FLUCTUATIONS

1. Air Showers

Electrons and photons in the atmosphere can contribute to the burst rate observed below 142 g cm^{-2} of lead. Crudely this contribution can be divided into two parts: In the first place, single electrons or photons of sufficient energy will initiate a cascade capable of penetrating the lead and producing the required burst; and secondly, extensive air showers with a very high density of particles will still contain enough electrons under the shield to produce the required ionization in the chamber. We have computed the ionization burst rate due to single electrons and photons by extrapolating the energy spectrum of high energy electrons and photons reported by Rossi[33,34] and found a value approximately 3×10^{-3} times the observed AIB rate either at sea level or at 10,600 feet. A calculation using the method developed by Greisen[35] shows that the burst rate caused by dense air showers is approximately 3×10^{-5} times the observed AIB rate either at sea level or at 10,600 feet. If the additional requirement that a counter in tray C be struck is imposed, these values are further reduced. These results are, of course, only correct as to order of magnitude. They indicate, however, that if air showers consisted of electrons and photons exclusively, the number of bursts associated with air showers should be exceedingly small.

In order to test this point experimentally, we performed at 10,600 feet an experiment with essentially the same experimental arrangement as in Fig. 1, except for an additional tray of Geiger counters of 0.15 square meters placed 3 meters from the detector and at the same height as the lower counter in tray B. With no absorber above tray A and with 171 g cm^{-2} of lead between tray A and the ionization chamber (rather than 142 g cm^{-2} as shown in Fig. 1), (5.4±0.5) percent of the $AI_{0.3}B$ events were associated with discharges in the extension shower tray. When the amount of lead between tray A and the ionization chamber was increased to 285 g cm^{-2}, (5.0±0.6) percent of the $AI_{0.3}B$ events were associated with discharges in the

[30] Camerini, Davies, Fowler, Franzinetti, Lock, Perkins, and Yekutieli, Phil. Mag. **42**, 1261 (1951).
[31] L. S. Osborne, Phys. Rev. **81**, 239 (1951).
[32] Cocconi, Cocconi Tongiorgi, and Widgoff, Phys. Rev. **79**, 768 (1950).
[33] B. Rossi, Revs. Modern Phys. **21**, 104 (1949).
[34] Approximation B of the shower theory in B. Rossi and K. Greisen, Revs. Modern Phys. **13**, 240 (1941), has been used in these calculations.
[35] K. Greisen, Phys. Rev. **75**, 1071 (1949).

extension shower tray. In absolute value, the $AI_{0.3}B$ coincidence rate associated with air showers was reduced in the ratio of 1 to 0.70±0.11 when 114 g cm^{-2} of lead were added to the 171 g cm^{-2} of lead between tray A and the ionization chamber.

This small decrease, together with the large discrepancy between the computed and observed numbers of AIB events associated with air showers, shows conclusively that the events cannot be explained by the electronic component of air showers alone. Most likely they are mainly caused by the simultaneous arrival upon the instrument of N-rays and electrons, as part of the same air shower.[36] The electrons discharge the extension tray, whereas the N-rays through their nuclear interactions give rise to the AIB coincidences as in the case of unassociated events.

An experiment similar to the one described above but performed at sea level showed that 5 percent of the $AI_{0.6}$ events were associated with extensive air showers. All of the associated events contained particles of sufficient penetrating power to discharge several counters in tray C under an additional 171 g cm^{-2} of lead.

2. Barometric Effect

The data of the experiments reported here have not been corrected for the fluctuations in the barometric pressure.[37] At 10,600 feet the maximum variation of pressure during the time of the experiment was 12 g cm^{-2}. This pressure change should cause a variation of about 10 percent in the intensity of the N-rays since according to our measurements, the absorption thickness of the N-rays in air is 119 g cm^{-2}. Each measurement, with the exception of the one taken with no absorber above tray A, was run for at least two weeks and none of the severe barometric disturbances lasted more than a few days during the time of the experiment. Thus, the coincidence rates from all measurements (with the possible exception of the measurement with no absorber) should have errors much less than 10 percent from barometric fluctuations.

The authors are greatly indebted to Professor Bruno Rossi for his aid in planning this experiment and for his advice and criticism during the analysis of the results. They wish to thank Mr. Seymour Weiner who helped in performing the experiment at sea level and Mr. Daniel Anderson who did similarly at 10,600 feet. The facilities of the Inter-University High Altitude Laboratory were invaluable, and the aid of Professor Cohn and Professor Iona of the University of Denver was appreciated.

APPENDIX

In order to evaluate the contribution of μ-meson induced bursts to the total burst rates we have attempted to calculate the rate of μ-meson induced bursts at sea level and 10,600 feet. That is, we have tried to determine the number of μ-mesons which could produce, by electromagnetic interactions in the lead above the ionization chamber, electrons or photons capable of initiating the electron showers which cause the bursts.[38] These calculations have been perforce very approximate because of the limitations of present theories regarding the probability for electromagnetic interactions of μ-mesons, because of the difficulty in treating an electron cascade developing partly in lead and partly in air, and because we have neglected fluctuations from average shower behavior.

Neglecting fluctuations, the rate of ionization bursts induced by the μ-mesons is

$$n=\int_0^T dt\int_{E_{\min}(E'')}^{\infty} N_\mu(E)dE\int_{E''(t)}^{E_{\max}'(E)} P(E,E')dE', \quad (1)$$

where t is the number of radiation lengths above the chamber at which the interactions take place, $N_\mu(E)dE$ is the differential number energy spectrum in the vertical direction of μ-mesons,[39] and $P(E,E')dE'$ is the probability per radiation length for a meson of energy E to produce an electron or photon of energy E' in dE'. This yields for n the total number of bursts per second, per cm^2, and per steradian in the vertical direction. The minimum burst size which contributes to n is determined by the limits of the integration of Eq. (1). $E_{\max}'$ is the maximum energy which a μ-meson of kinetic energy E can transfer to an electron or photon, and $E_{\min}(E'')$ is the minimum kinetic energy a μ-meson must have in order to produce an electron or photon of kinetic energy E''. E'' is the minimum energy an electron or photon produced at thickness t of lead above the chamber must possess in order to initiate an electronic shower which will trigger the ionization chamber. The minimum detected ionization burst, $I_{0.3}$, corresponded to 16 minimum ionizing particles traversing the chamber perpendicular to its axis.

Experimental and theoretical results[40,41] show that because of large angle scattering in the lead, not all the electrons in an electronic shower will emerge from the lead and traverse the ionization chamber. In the experiments of this paper an ionization chamber which had a brass wall 0.081 cm thick and was 7.5 cm in diameter and 52 cm long was placed in a cavity in the

[36] Cocconi, Cocconi Tongiorgi, and Greisen, Phys. Rev. **75**, 1063 (1949).

[37] With the exception of the "coherence experiment" as has been noted.

[38] The number of ionization bursts produced by μ-mesons at sea level has been computed by R. F. Christy and S. Kusaka, Phys. Rev. **59**, 414 (1941). The present calculation is for smaller bursts than those considered by Christy and Kusaka. It is for vertically incident mesons on an infinite plane geometry and has been carried out for two elevations, while Christy and Kusaka's calculations are for spherical geometry at sea level. There are salient differences in the two methods of calculation for which the reader is referred to the above article.

[39] $N_\mu(E)$ was assumed independent of the thickness, t, at which the interaction occurred.

[40] S. N. Vernov and O. N. Vavilov, Phys. Rev. **70**, 769 (1946); Blocker, Kenny, and Panofsky, Phys. Rev. **79**, 419 (1950).

[41] R. R. Wilson, Phys. Rev. **86**, 261 (1952).

lead 16 cm×30.5 cm×83 cm. In what follows we have assumed that the lead to air boundaries and the chamber wall reduce the number of shower electrons at the ionization chamber to one-half the number that would be present if the shower developed in lead alone. Thus, a 32-electron shower at the position of lead boundary will be assumed to produce the minimum detected ionization burst and proportionally higher numbers of electrons will be required for the larger size bursts.

In dealing with the development of electronic showers in the lead we have used "Approximation B" of the shower theory in Rossi and Greisen.[42] This approximation is poor for lead because of the breakdown at small energies of the asymptotic formulas for radiation phenomena and pair production which are used in this approximation. Belenky, using the proper cross section for pair production at lower energies, has computed the position of the shower maxima and the number of particles at the maxima for showers initiated by electrons or photons of different energies.[6] He has, however, assumed that the number of particles in a shower is a Gaussian function of the distance from the shower maximum. This assumption is obviously very poor except very close to the shower maximum. It overestimates the number of shower particles at small thicknesses, and it greatly underestimates the number of shower particles at large thicknesses. Therefore, we have used "Approximation B" in preference to the theory given by Belenky.

Figure 14 shows the minimum energy, E'', that an electron must possess to initiate at a thickness t above the ionization chamber a cascade which will produce an $I_{0.3}$ burst. $E''(t)$ can be approximated in the region $2<t<\infty$ by the expressions

$$\begin{aligned} E''&=40e^{-0.77t} \quad \text{for} \quad 2\leq t<4.5,\\ E''&=0.5e^{+0.22t} \quad \text{for} \quad 4.5\leq t<\infty,\\ E_{\min}''&=1.25 \quad \text{for} \quad t=4.5, \end{aligned} \tag{2}$$

as indicated by the dashed lines in Fig. 14. $E''(t)$ is in Bev and t is in radiation lengths. We have assumed in our calculations that $E''(t)$ is identical for photon and electron initiated showers. The errors introduced by this assumption are small because we are interested only in showers that contain at least 32 electrons. A considerable discrepancy exists between the values of $E_{\min}''$ (E'' for t equal to the depth of the shower maximum) obtained using "Approximation B" and the values obtained from the computations of Belenky. As stated in the introduction, the value of $E_{\min}''$ from Belenky is about 3.2 Bev and occurs at about 48 g cm^{-2} of lead above the chamber. The value of $E_{\min}''$ from "Approximation B" is about 1.50 Bev and occurs at about 30 g cm^{-2} of lead above the chamber.[43] This discrepancy again indicates that the results of our calculation will be approximate.

If we substitute E'' for t as the variable of integration, neglect electronic showers initiated in the first two radiation lengths of lead above the ionization chamber, and assume the lead above the chamber to be of infinite thickness, Eq. (1) becomes, for $I_{0.3}$ bursts,

$$\begin{aligned} n=&\int_{1.25}^{\infty}(dt/dE'')dE''\int_{E_{\min}(E'')}^{\infty}N_\mu(E)dE\\ &\times\int_{E''}^{E_{\max}'(E)}P(E,E')dE'+\int_{8.6}^{1.25}(dt/dE'')dE''\\ &\times\int_{E_{\min}(E'')}^{\infty}N_\mu(E)dE\int_{E''}^{E_{\max}'}P(E,E')dE'. \end{aligned} \tag{3}$$

The limits for E'' are in Bev. Since t is a doubled-valued function of E'' with a minimum at $t=4.5$ radiation lengths, Eq. (3) is the sum of two terms. The first term includes the electronic showers initiated at thicknesses greater than 4.5 radiation lengths above the chamber in which case $dt/dE''=4.6/E''$. The second term includes the electronic showers initiated at thicknesses between 2 and 4.5 radiation lengths above the chamber in which case $dt/dE''=-1.3/E''$. The error introduced both in neglecting showers initiated in the first two radiation lengths of lead and in assuming the

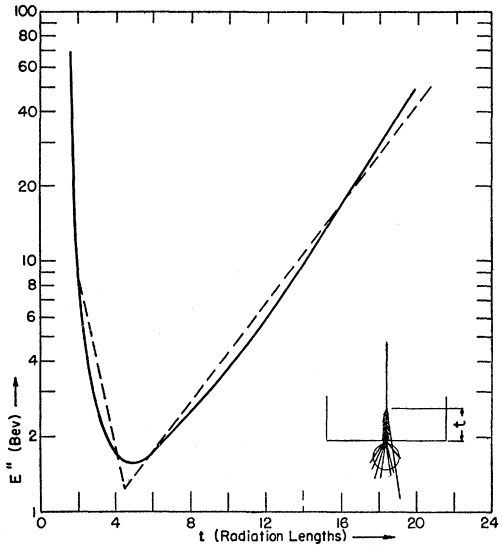

FIG. 14. The electron energy, E'', necessary to initiate at a thickness t of lead above the chamber an electronic cascade which will contain at least 32 electrons in the lead directly above the chamber [after Rossi and Greisen (see reference 42)].

[42] B. Rossi and K. Greisen, Revs. Modern Phys. **13**, 240 (1941).

[43] Including the effects of multiple scattering, Wilson has recently applied the Monte Carlo method to the problem of cascade showers in lead. For showers initiated by 500 v Mev photons or electrons, his determination of the depth of the shower maximum agrees more closely with "Approximation B" than with the results of Belenky. Wilson's results indicate that our use of "Approximation B" with the assumption that one-half the shower electrons do not contribute to the ionization in the chamber is a good approximation to the correct shower behavior (see reference 41).

lead above the chamber to extend to infinity is very small.

In order to more easily evaluate the triple integrals of Eq. (3), we wished to integrate last over the differential μ-meson spectrum, $N_\mu(E)$, which could not easily be expressed in analytical form. This required interchanging the order of integration between the variables E and E''. Figure 15 shows the areas of integration in the E, E'' plane for the two terms in Eq. (3). In order to interchange the order of integration the second term in Eq. (3) had to be broken into the sum of two terms. Equation (4) is the equation used in the computation to determine the $I_{0.3}$ ionization bursts due to μ-mesons:

$$n=\int_{E(E''=1.25)}^{\infty} N_\mu(E)dE\int_{1.25}^{E_{\max}''(E)}(4.6/E'')dE''$$
$$\times\int_{E''}^{E_{\max}'(E)}P(E,E')dE'+\int_{E(E''=8.6)}^{E(E''=1.25)}N_\mu(E)dE$$
$$\times\int_{E_{\max}''(E)}^{1.25}-(1.3/E'')dE''\int_{E''}^{E_{\max}'(E)}P(E,E')dE'$$
$$+\int_{E(E''=8.6)}^{\infty}N_\mu(E)dE\int_{8.6}^{1.25}-(1.3/E'')dE''$$
$$\times\int_{E''}^{E_{\max}'(E)}P(E,E')dE'. \quad (4)$$

Similar equations were obtained for the $I_{0.6}$ and $I_{1.2}$ bursts due to μ-mesons. We used the expressions for $E''(t)$ given in Eq. (2) multiplied by a factor of 2 for the $I_{0.6}$ bursts and multiplied by a factor of 4 for the $I_{1.2}$ bursts.

The differential μ-meson spectrum, $N_\mu(E)$, and the probability for μ-mesons to produce electrons and photons by electromagnetic interactions have yet to be discussed. Since our detector selected nearly vertical rays, the differential energy spectrum of vertically incident μ-mesons was used. For energies in the region 1 to 7 Bev the energy spectrum was derived from the differential range spectrum at sea level reported by Rossi.[44] Beyond this point we used the same differential spectrum as that used by Christy and Kusaka.[38] Over the range 1 to 50 Bev the spectrum we used agrees very well with the recent results of Caro, Parry, and Rathgeber,[45] and beyond 50 Bev can be represented by a power law $kE^{-2.9}$. The energy spectrum at 10,600 feet was obtained from the sea level spectrum. We used the survival probabilities computed by Sands[46] to account for those μ-mesons which decay in traversing the 310 g cm^{-2} of air from 10,600 feet to sea level. We neglected the production of burst-producing μ-mesons (energy over 1.25 Bev) between 10,600 feet and sea level.

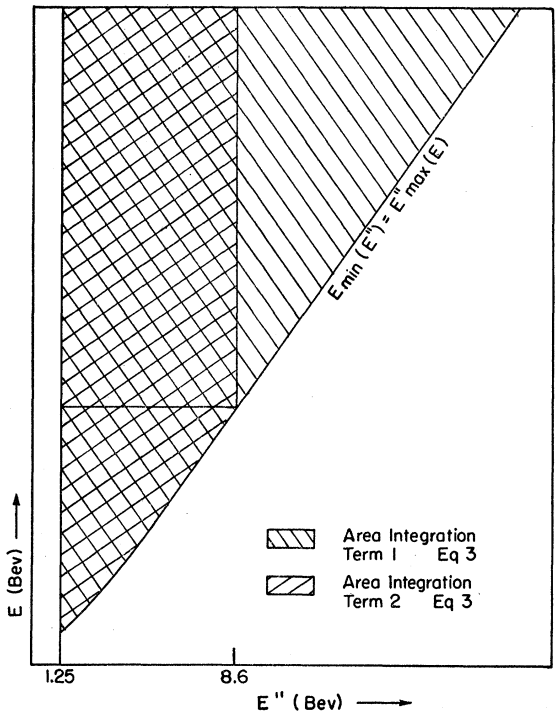

FIG. 15. The area of integration in the E, E'' plane. E is the energy of a μ-meson and E'' the minimum energy of an electron or photon required to initiate a burst-producing shower.

There are three known types of electromagnetic interactions in which μ-mesons can produce high energy electrons or photons. These are collisions with atomic electrons, radiation processes in the field of nuclei and atomic electrons, and pair production in the field of nuclei and atomic electrons. The probabilities for μ-mesons to produce high energy electrons by collision and to produce high energy photons by radiation are well known.[47] No general formula is available, however, for the production of high energy electron pairs by charged particles. Hayakawa[48] has shown under simplifying assumptions that the energy lost by μ-mesons of the energy under consideration in pair production is of the same order as that lost in radiation processes. Davisson,[49] however, has shown that in pair production as compared to radiation processes, a considerably greater percentage of the energy loss is in small energy transfers. We have neglected pair production by μ-mesons in the calculation.

We made the following approximations in computing the probabilities for radiation and collision of μ-mesons

[44] B. Rossi, Revs. Modern Phys. **20**, 537 (1948).
[45] Caro, Parry, and Rathgeber, Australian J. Sci. Research **A4**, 16 (1951).
[46] M. Sands, Tech. Report No. 28, LNSE, Massachusetts Institute of Technology (1949).
[47] See probabilities for particles of spin $\frac{1}{2}$ in B. Rossi and K. Greisen, Revs. Modern Phys. **13**, 240 (1941).
[48] S. Hayakawa, Prog. Theoret. Phys. **4**, 287 (1949).
[49] R. J. Davisson, private communication to B. Rossi.

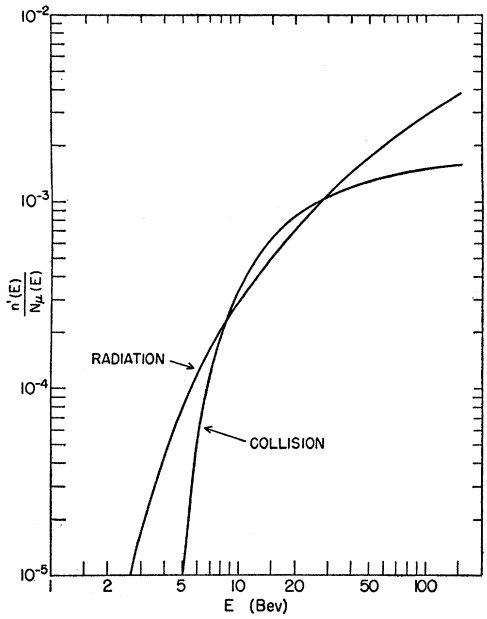

FIG. 16. The probability that an $I_{0.3}$ burst be produced by a μ-meson of energy in dE at E as a function of μ-meson energy.

assumed to have spin $\frac{1}{2}$:

$$mc^2=0.1, \quad p^2c^2 \gg m^2c^4, \tag{5}$$

where m is the mass and p is the momentum of the μ-meson, and all energies are in Bev.

With these approximations we obtained for the probability of collision processes per radiation length

$$P_{\text{col}}(E, E')dE'=3.9\times10^{-4}\left(\frac{1}{E'^2}-\frac{10+E}{E'E^2}+\frac{1}{2E^2}\right)dE'. \tag{6}$$

For collision processes, $E_{\max}'$ is given by

$$E_{\max}'(E)=E_{\max}''(E)=E^2/(10+E). \tag{7}$$

Similarly, the probability of radiation processes per radiation length is

$$P_{\text{rad}}(E, E')dE'$$
$$=9.8\times10^{-6}\left\{\left[\frac{3}{4}\frac{E'}{(E+0.1)^2}+\frac{1}{E'}-\frac{1}{(E+0.1)}\right]\right.$$
$$\left.\times\left[\ln 5.5(E+0.1)(E+0.1-E')/E'-\tfrac{1}{2}\right]\right\}dE'. \tag{8}$$

For radiation processes the maximum transferable energy $E_{\max}'=E_{\max}''$, defined as the value of E' for which P_{rad} goes to zero, is slightly smaller than the μ-meson kinetic energy, E.

Since the limits of integration were different in the two cases, Eq. (4) had to be evaluated separately for collisions and radiation processes of μ-mesons. In evaluating Eq. (4) for the bursts induced by collision processes of μ-mesons, the first two integrations in each of the three terms were performed analytically, while the third integration was performed graphically. For the bursts due to radiation processes of μ-mesons, however, the triple integrals were evaluated numerically.

The probability for a μ-meson of energy E to cause an ionization burst was obtained as an intermediate step in the calculation. In the case of $I_{0.3}$ bursts, this probability for both radiation and collision processes is shown in Fig. 16. The curves of Fig. 16, which are the weighting factors for the differential μ-meson spectrum in calculating the number of $I_{0.3}$ bursts, give an indication of the errors involved in the commonly used assumption that μ-mesons above a certain energy contribute with equal weight to producing bursts, while μ-mesons below this energy do not contribute at all to the bursts.

Figure 17 shows the μ-meson spectrum at sea level weighted by the curves of Fig. 16. This figure gives the burst rate per unit energy interval as a function of the μ-meson energy. Integration of the curves of Fig. 17 gives the $I_{0.3}$ μ-burst rate at sea level.

Table IX shows the final results of calculations for sea level and 10,600 feet for three different values of minimum ionization chamber pulse.[50] From the results in this table we see that for the $I_{0.3}$ bursts induced by μ-mesons incident in the vertical direction, the increase from sea level to 10,600 feet is in the ratio of 1.00 to 1.20.

This increase in the rate of μ-bursts from sea level to 10,600 feet has been used in Sec. III.3 to separate the μ-bursts from N-bursts. While the absolute values of the burst rate due to μ-mesons calculated as described above may be in considerable error, the increase in the burst rate between sea level and 10,600 feet should be much more reliable, because the effects of many of the approximations made in computing the absolute values tend to cancel out when the ratio of these numbers is taken.

Indeed, the results for the μ-meson separation at sea level in Sec. III.3 do not depend critically on the altitude variation of the rate of μ-bursts. Assuming that no error was involved in the computation of the altitude variation of the μ-bursts, we have computed that (51±4) percent of the bursts at sea level are N-bursts. This percentage would be (52±4) if the burst producing μ-mesons did not increase with altitude and would be (48±4) if their intensity doubled between the two elevations. This percentage is, however, strongly dependent on the altitude variation of the N-bursts. In our calculation we assumed that the altitude variation of the $I_{0.3}$ N-bursts was identical to the altitude variation of the $AI_{0.3}BC_2$ events, which corresponded to an absorption thickness in air of 119 g cm^{-2}. We

[50] If we convert these values of n to those which correspond to a $\cos^2\theta$ dependence of the meson intensity about the zenith and to 2π solid angle, they can be compared with the values of Christy and Kusaka for bursts of 100 particles. The agreement is good.

could also have used the absorption thickness for N-bursts of similar size determined from measurements with similar detectors at elevations where the μ-bursts can be neglected.[4] If we take as a lower limit for the absorption thickness 110 g cm^{-2} and as an upper limit 125 g cm^{-2} we find the percentage of bursts due to nuclear interactions at sea level varies between the limits of 41 and 60 percent.

Since for the AIB events the number of μ-bursts is comparable with the number of N-bursts at sea level, and therefore can be neglected in comparison with the number of N-bursts at 10,600 feet, the integral burst size frequency distribution, $(N(E)=kE^{-\gamma})$, at 10,600 feet with $\gamma=1.4$ represents to a first approximation the N-bursts alone. At sea level the size frequency distribution is a power law with $\gamma\approx1.8$ and represents a mixture of μ-bursts and N-bursts. In order to explain the observed change with altitude in the distribution function without assuming a change in the distribution function of N-bursts, one would have to approximate the distribution of μ-bursts at sea level by a power law with $\gamma\approx2.5$. However, the results of our calculation

TABLE IX. The ionization burst rate in cm^{-2} sterad^{-1} sec^{-1} at sea level and 10,600 feet resulting from radiation and collision processes of μ-mesons.

Minimum pulse height	$I_{0.3}$	$I_{0.6}$	$I_{1.2}$
Sea level			
Radiation	6.55×10^{-7}	2.59×10^{-7}	0.932×10^{-7}
Collision	5.33×10^{-7}	1.24×10^{-7}	0.273×10^{-7}
Total	11.88×10^{-7}	3.83×10^{-7}	1.205×10^{-7}
10,600 ft			
Radiation	7.78×10^{-7}	3.08×10^{-7}	1.059×10^{-7}
Collision	6.46×10^{-7}	1.45×10^{-7}	0.307×10^{-7}
Total	14.24×10^{-7}	4.53×10^{-7}	1.366×10^{-7}

given in Table IX indicate an integral pulse-height distribution for μ-bursts with $\gamma=1.6$.

This value could only be increased significantly if the production of bursts by collision processes predominated over the production of bursts by radiation processes for μ-meson energies where the μ-meson spectrum is steep. The larger bursts are produced by μ-mesons of energies where the μ-meson spectrum is steep but are produced mainly by radiation processes (see Table IX). Collision processes are important in producing the smaller bursts, but these bursts are mainly produced by μ-mesons of energies where the μ-meson spectrum has begun to flatten off.[51]

In Sec. III.3 we have determined the rate of $AI_{0.3}B$

[51] Because of the nature of Eq. (4) it is difficult to discuss quantitatively the effects of the various parameters. However, assuming that direct pair production by μ-mesons can be neglected, the relative contribution to n by collision and radiation processes depends on the relative radiation and collision probabilities as a function of energy and on the shape of the μ-meson spectrum. We have carried out the calculations with two other spectra, and as long as the meson spectrum does not fall off much faster than we have assumed above, the pulse-height distribution cannot be much steeper than given by our calculation.

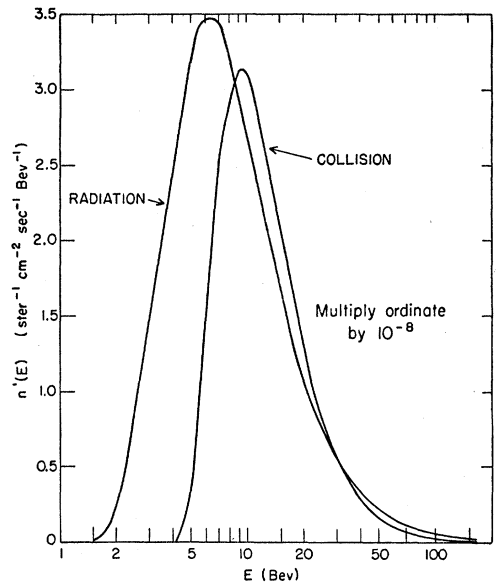

FIG. 17. The number of $I_{0.3}$ bursts contributed by radiation and collision processes per energy interval as a function of μ-meson energy. $n'(E)=dn/dE$ where n has the usual significance and E is the μ-meson energy.

bursts caused by μ-mesons. Table IX gives the calculated burst rate per sterad cm^2 sec for the $I_{0.3}$ bursts caused by μ-mesons. From these data we have determined the effective "area-solid angle product" for our detector to be 183 sterad cm^2.

From this effective "area-solid angle product" of the ionization chamber and from the $AI_{0.3}B$ rate due to the N-component, we can roughly calculate the intensity of the charged burst producing N-rays incident from the atmosphere at sea level and at 10,600 feet. For this calculation we have assumed that the N-bursts are caused by electronic cascades which are initiated by single photons arising from nuclear interactions. Equation (9) gives the number n_P of bursts resulting from interactions of the protons which constitute the charged N-component in the atmosphere. These bursts will be called proton bursts:

$$n_P=\int_0^T dt\int_{E(E'')}^{\infty} N_P(E)dE\int_{E''(t)}^{E_{\max}'} P_P(E,E')dE'. \quad (9)$$

In Eq. (9) $N_P(E)$ is the differential number energy spectrum in the vertical direction of protons in the atmosphere, and $P_P(E,E')$ is the probability for a proton of kinetic energy E to cause an interaction from which the kinetic energy E' appears in the electronic component. The terms used in Eq. (9) are defined in identical manner as the similar terms in Eq. (1) except they are for protons and proton bursts, rather than μ-mesons and μ-bursts.

The last integral in Eq. (9) is just the probability for a proton of energy E to produce a burst. For protons above the energy $E(E'')$ we have assumed that this

probability is (1/167) g^{-1} cm^2 or 1/25.6 per radiation length, which is the interaction probability corresponding to the geometrical cross section in lead. We have used a proton energy spectrum of $aE^{-2.5}$ for the energy region in question, and have assumed that the protons are absorbed in the lead with an absorption thickness of 195 g cm^{-2},[52] (30 radiation lengths) independent of energy.

If we substitute the above values and the values of $E''(t)$ from Eq. (2) into Eq. (9) and if we neglect, as we have done for the μ-bursts, electronic showers initiated in the first two radiation lengths of lead, we obtain for the case where absorber Σ' alone is present:

$$n_P=\frac{1}{25.6}\int_2^{4.5} dt \times\int_{E(E''=40\exp[-0.77t])}^{\infty}\left[aE^{-2.5}\exp\left(-\frac{33.6-t}{30}\right)\right]dE + \frac{1}{25.6}\int_{4.5}^{33.6} dt \times\int_{E(E''=0.5\exp[+0.21t])}^{\infty}\left[aE^{-2.5}\exp\left(-\frac{33.6-t}{30}\right)\right]dE, \tag{10}$$

where t is the distance in radiation lengths from the ionization chamber.

In order to evaluate Eq. (10), we have assumed $E(E'')$ (which is the minimum kinetic energy that a proton must possess in order to transfer an energy E'' into the electronic cascade) to be a constant b times E''. Upon integration Eq. (10) becomes

$$n_P=0.030a/b^{1.5}. \tag{11}$$

If we assume that one-third of the proton kinetic energy goes into the electronic cascade, $b=3$, the number of bursts in $sterad^{-1}$ cm^{-2} sec^{-1} becomes

$$n_P=5.7\times10^{-3}a. \tag{12}$$

This calculated value of n_P can be compared with an experimentally measured value to determine a, and we can then calculate the absolute proton intensity in the atmosphere. Unfortunately, the experimental value of n_P must be obtained from the rate of N-bursts which we cannot relate simply to the rate of proton bursts; i.e., the absorption curves cannot be uniquely extrapolated to zero thickness. We assumed that one-half the AIB events observed with Σ' alone above the detector were proton bursts. Using the effective "area-solid angle product" we find

$$\begin{aligned} n_P&=6\times10^{-7}\ \text{sterad}^{-1}\ \text{cm}^{-2}\ \text{sec}^{-1} \quad \text{at sea level,}\\ n_P&=9\times10^{-6}\ \text{sterad}^{-1}\ \text{cm}^{-2}\ \text{sec}^{-1} \quad \text{at 10,600 feet.}\end{aligned} \tag{13}$$

From Eqs. (12) and (13) one obtains the following absolute value for the proton spectrum in the atmosphere:

$$\begin{aligned} N_P dE&=1.05\times10^{-4}E^{-2.5}dE \quad \text{at sea level,}\\ N_P dE&=1.6\times10^{-3}E^{-2.5}dE \quad \text{at 10,600 feet,}\end{aligned} \tag{14}$$

where N_P is in $sterad^{-1}$ cm^{-2} sec^{-1} Bev^{-1} and E is in Bev.

In spite of the many approximations and assumptions we have made in the calculation of the proton intensity, our results agree as to order of magnitude with results previously reported.[53,54] We have assumed that we detect protons of energy above 3.75 Bev. At 10,600 feet Eq. (14) yields at $E=4$ Bev, for N_P, 5×10^{-5} $sterad^{-1}$ cm^{-2} sec^{-1} Bev^{-1}. This compares with the value of 7×10^{-5} $sterad^{-1}$ cm^{-2} sec^{-1} Bev^{-1} for N_P at 4 Bev determined by Whittemore and Shutt at 11,200 feet with a cloud-chamber experiment. Our results also agree with theirs in that at 10,600 feet we find that 5 percent of the charged particles of energy above 4 Bev are protons. At sea level our results are in agreement with those of Mylroi and Wilson, who obtained for the proton spectrum in the range 1–10 Bev/c, $N_P dp=1.0\times10^{-4}p^{-2.8}dp$, where p is the momentum in Bev/c and N_P is in $sterad^{-1}$ cm^{-2} sec^{-1} $(Bev/c)^{-1}$.

[52] Using the model of the semitransparent nucleus, the absorption thickness in lead was calculated from the absorption thickness of 119 g cm^{-2} in air. The "transition effect" in the absorption of the N-component, which obviously contradicts this absorption thickness in lead, was assumed in Sec. III.4 to be due to causes other than the absorption of the protons from the atmosphere.

[53] W. L. Whittemore and R. P. Shutt, Phys. Rev. **86**, 940 (1952).

[54] M. G. Mylroi and J. G. Wilson, Proc. Phys. Soc. (London) **A64**, 404 (1951).